Water-Based Oxygen-Sensor Films

Arezoo Habibagahi,[†] Youssef Mébarki,[‡] Yasir Sultan,[†] Glenn P. A. Yap,[§] and Robert J. Crutchley*,[†]

Ottawa-Carleton Chemistry Institute, Carleton University, Ottawa, Ontario K1S 5B6, Canada, Institute for Aerospace Research, National Research Council of Canada, Ottawa, Ontario K1A 0R6, Canada, and Department of Chemistry & Biochemistry, University of Delaware, Newark, Delaware 19716

ABSTRACT The luminescent cyclometalated iridium complex $[Ir(fppy)_2(t\text{-Bu-iCN})_2]CF_3SO_3$, **1** (fppy = 4-(2-pyridyl)benzaldehyde, and *t*-Bu-iCN = *tert*-butyl isocyanide), was synthesized and characterized by X-ray crystallography and ^{1}H NMR, absorption, and emission spectroscopies. Complex **1** was quantitatively bound to the water-soluble amine-functionalized polymer Silamine D208-EDA by reductive amination, to produce **2**. The quantum yield of emission and excited state lifetime of **2** ($\phi_{em} = 0.23$ and $\tau = 20.6\ \mu s$) are comparable to that of the model complex $[Ir(tpy)_2(t\text{-Bu-iCN})_2]CF_3SO_3$, **3** (tpy = 2-(*p*- tolyl) pyridine) with $\phi_{em} = 0.28$ and $\tau = 35.6\ \mu s$. Aqueous blends of **2** with Silamine and colloidal microcrystalline cellulose (MC) were used to prepare oxygen-sensor films. Oxygen sensitivities of these films were determined as a function of Silamine:MC ratio and obeyed Stern−Volmer kinetics. The optimum oxygen-sensor film composition was **2** in 1:1 Silamine:MC, which had an oxygen sensitivity of 0.502 over an atmospheric pressure range of 0.007−45 psi. Temperature sensitivity (percentage loss of intensity per °C) of this film was determined to be −1.1 and −1.4% °C^{-1} at vacuum and 1 bar atmospheric pressure, respectively. These results were compared to those of films incorporating dispersions of **1** and **3**. Luminescence microscopy of 9:1, 1:1, and 1:5 Silamine:MC films of **2** show that the charged iridium complex in **2** associates with the surface of MC and lifetime measurements of these films show an increase in lifetime with increasing MC fraction. The optimum quenching sensitivity observed for the 1:1 Silamine:MC film suggests that the diffusion of oxygen must decrease with increasing fraction of MC and thereby decrease oxygen sensitivity. These novel materials offer an environmentally friendly alternative to the preparation of oxygen-sensor films.

KEYWORDS: Pressure-sensitive paints • barometry • iridium luminescence • quenching • oxygen-sensor films, • luminescent polymers

INTRODUCTION

Research in optical oxygen sensors has found application in a variety of fields including in vivo imaging (1, 2), aerodynamics (3–5), environmental analysis (6–8), analytical chemistry (9 −11), food industry (12, 13), and biochemistry (14–21). In the field of aerodynamics, oxygen-sensor materials are incorporated in pressure-sensitive paint (PSP) formulations, the films of which are sensing materials whose photophysical properties change with changing air pressure (3, 5, 22–40). PSP formulations in current use are based in organic solvents and, because of their volatile organic content, their application and recycling engender workplace safety and contamination concerns. These concerns could be eliminated by using an entirely aqueous PSP formulation that possesses acceptable performance compared to commercial PSPs. Oglesby and Ingram developed a water-based PSP that incorporated nonvolatile organic solvents, an emulsion polymer and a platinum porphyrin luminescent compound (41). This PSP formulation showed good performance in a low pressure range (0 to 15 psi); however, the main disadvantage of emulsions is that they are prone to phase separation without an organic stabilizer and thus require greater care in their application than homogeneous formulations. It was therefore desirable to create a homogeneous formulation that is entirely water based.

In past research (4, 42–44), we have used luminescent iridium complexes in PSPs because of their large quantum yields of emission and sensitivity to oxygen. These iridium complexes possess poor solubility in aqueous solution but, as this study will show, covalent attachment to a water-soluble polymer is a solution to this problem. We report the synthesis and characterization of $[Ir(fppy)_2(t\text{-Bu-iCN})_2]CF_3SO_3$, **1**, where fppy = 4-(2-pyridyl)benzaldehyde and *t*-Bu-iCN is *t*-butyl-isocyanide. In situ reductive amination with methanolic pyridine-borane (45) presents a conveniently mild process for covalent attachment of the carbonyl functionalized complex to the water-soluble amine functionalized polymer Silamine D208-EDA to produce the water-soluble strongly luminescent material **2**. The photophysical properties of **1** and **2** are similar to $[Ir(tpy)_2(t\text{-Bu-iCN})_2]CF_3SO_3$, **3**, where tpy = N, C2′-(2-para-tolylpyridine), which possesses an excited state lifetime of $\tau = 35.6\ \mu s$ and emission quantum yield of $\Phi = 0.28$ (46). Aqueous blends of **2** with Silamine and colloidal microcrystalline cellulose (MC) were used to prepare oxygen-sensor films whose properties were determined over an atmospheric pressure range of 0.007−45 psi. These results were compared to those of films incorporating dispersions of **1** and **3**, and the results indicate that

* Corresponding author.
Received for review May 7, 2009 and accepted July 9, 2009
† Carleton University.
‡ National Research Council of Canada.
§ University of Delaware.
DOI: 10.1021/am900306a

films of **2** are efficient barometric sensors for wind tunnel applications.

EXPERIMENTAL SECTION

Materials. Iridium(III) chloride hydrate (Pressure Chemical), 2-(*p*-tolyl)pyridine (tpy) (Aldrich), 4-(2-pyridyl)benzaldehyde (fppy) (Aldrich), silver trifluoromethanesulfonate (AgOTf) (Aldrich), tert-butyl isocyanide (CN-*t*-Bu) (Aldrich), colloidal microcrystalline cellulose (Aldrich), and pyridine-borane (Aldrich) were used as received. Silamine D208 EDA (MW 2475, amine value 30) was purchased from Siltech Corp. and heated to 80 °C under vacuum for 30 min before use. 2-Ethoxyethanol (ReagentPlus, Aldrich) was distilled and dried over $MgSO_4$ (Aldrich). Dichloromethane (Technical, ACP chemicals) was dried over calcium hydride (Aldrich) and distilled and stored under argon before use. Methanol (HPLC grade, J. T. Baker) and diethyl ether (Anhydrous ACS, Fisher Scientific) were used as received. For the reductive amination reaction, dichloromethane (Spectro grade, Caledon, 24 mL) was dried over activated 4 Å molecular sieves (0.53 g) overnight. For spectroscopy, acetonitrile (Spectrograde, Fisher Scientific) and dichloromethane (Spectro grade, Caledon) were used as received. The complex $[Ir(tpy)_2(CN\text{-}t\text{-}Bu)_2](CF_3SO_3)$ was synthesized using the method of Li et al. (45), and the dimer complex $[Ir(fppy)_2Cl]_2$ was prepared according to Lo et al. (47).

Spectroscopic Measurements. Absorption and steady-state emission spectra were acquired in Spectrograde acetonitrile and dichloromethane on a Cary 5 UV−vis-NIR spectrophotometer and a Shimadzu RF-1501 spectrofluorophotometer, respectively, at ambient temperatures. To obtain time-resolved fluorescence decays, the samples were excited with the third harmonic of a Continuum Surelite 2 Nd:YAG laser generating pulses at 355 nm of 6 ns duration and 15 mJ energy. The signals from the monochromator/photomultiplier system were initially captured by a Tetronix TDS 2012 oscilloscope and transferred to a Macintosh PC clone computer with software LFP V3.0 developed in the LabVIEW environment from Luzchem. A total of 10 shots were averaged to obtain the decay traces. All solution lifetime experiments were done in static 1.0×1.0 cm^2 fused silica cuvettes, following purging with inert gas for 30 min. Each thin-film lifetime measurement was acquired on a plain microscope slide (Globe Scientific Inc.) sprayed with the paint using a conventional airbrush and mounted in a pressure chamber described elsewhere (43, 44). For the quantum yield determinations, the samples were optically matched to solutions of Coumarin 1 (Laser grade, Fisher) in ethanol ($\phi = 0.73$) (48) at room temperature using a Shimadzu RF-1501 spectrofluorophotometer. Dichloromethane was used as the solvent for all lifetime and quantum yield measurements. NMR spectra were acquired using a Bruker 300 spectrometer at ambient temperatures on $CDCl_3$ (Canadian Isotopes Limited) solutions and referenced to TMS. Elemental analysis was performed by Canadian Microanalytical Service, Ltd. of Delta, BC, Canada. All microscopy was performed in air. For luminescence microscopy, PSP films were sprayed on plain microscope slides (Globe Scientific Inc.). The luminescence images were observed using a confocal microscope Carl Zeiss LSM510 Meta (405 nm, 42.6% laser intensity) with an ECPlan-Neofluar 40x/1.30 Oil Dic M27 objective exciting at 405 nm and collecting image data at 505 nm. The observed images were analyzed with LSM510 V.4.0 SP2.

Synthesis of $[Ir(fppy)_2(t\text{-}Bu\text{-}iCN)_2]CF_3SO_3 \cdot CH_2Cl_2$, 1. $[Ir(fppy)_2Cl]_2$ (0.14 g, 0.12 mmol) was dissolved in dichloromethane (15 mL) and a solution of AgOTf (0.07 g, 0.27 mmol) in methanol (15 mL) was added. The reaction solution was stirred for 1 h and then filtered. To the orange filtrate was added CN-*t*-Bu (0.25 g, 3.0 mmol), and the resultant solution was stirred for 2 days at room temperature. The reaction mixture was evaporated to dryness under vacuum and the yellow product was filtered. Yellow cubic crystals were obtained by ether diffusion into a dichloromethane solution of the crude complex. Yield: 0.15 g, 72%. Elemental anal. Calcd as the monosolvated $C_{35}H_{34}IrN_4O_5F_3S \cdot CH_2Cl_2$, (%): C, 45.19; H, 3.79; N, 5.86. Found: C, 45.13; H, 3.78; N, 5.74. ^1H NMR ($CDCl_3$, 300 MHz, see Figure S1 in the Supporting Information for proton labeling scheme): 9.70 (Ald., 1H, s), 9.20 (N6, 1H, d, 5.7 Hz), 8.13 (N3,4, 2H, m), 7.82 (P3, 1H, d, 8.0 Hz), 7.69 (N5, 1H, td, 6.3 Hz), 7.53 (P4, 1H, dd, 8.0 Hz), 6.61 (P6, 1H, s), 1.37 (t-Bu, 9H, s) ppm.

Synthesis of 2 by Attachment of 1 to Silamine D208-EDA. To Silamine D208-EDA (1.5 g, 0.6 mmol, predried by heating at 80 °C under a vacuum for 30 min) was added dichloromethane (24 mL). The solution was degassed with argon for 10 min and then 0.53 g of activated 4 Å molecular sieves and **1** (0.09 g, 0.1 mmol) were added, followed by pyridine-borane (0.01 mL, 0.099 mmol). After the solution was stirred at room temperature under argon for 16 h, methanol (10 mL) was added and the resultant solution was treated with 6 N HCl (10 mL) for 15 min, and then pH was adjusted to 12 using concentrated aqueous NaOH solution. NaCl was precipitated by addition of diethyl ether (100 mL) and filtered off. The filtrate was solvent stripped and the residue dissolved in a small volume of acetone, which was filtered sequentially through 1.0 and 0.45 μm Gelman Acrodiscs. The filtered solution was added dropwise to rapidly stirred hexanes yielding a clear, yellow polymer fluid.

PSP Formulations. For the 1:1 Silamine:MC PSP formulations, a solution of 17 mg of $[Ir(fppy)_2(t\text{-}Bu\text{-}iCN)_2]CF_3SO_3$ in 7.3 mL MeOH was added to another solution that was prepared by mixing 0.5 g of Silamine D208-EDA in 2 mL of H_2O. The combined solutions were filtered through a 1.0 μm Gelman Acrodisc and then mixed with 0.5 g of microcrystalline cellulose in 20 mL of H_2O. PSP formulations with different Silamine:MC ratios were made by changing the proportions of the mixing solutions. PSPs having **3** as the luminophore were made in the same manner explained above. To prepare PSPs out of **2**, we used water in place of methanol to dissolve the luminophore.

X-ray Structural Determination of $1 \cdot 0.25(CH_2Cl_2)$. A crystal was mounted using viscous oil onto a glass fiber and cooled to the data collection temperature. Data were collected on a Brüker-AXS APEX CCD diffractometer with graphite-monochromated Mo Kα radiation ($\lambda = 0.71073$ Å). Unit-cell parameters were obtained from 60 data frames, 0.3° ω, from three different sections of the Ewald sphere. No symmetry higher than triclinic was observed and solution in the centrosymmetric space group option yielded chemically reasonable and computationally stable results of refinement. The data set was treated with SADABS absorption corrections based on redundant multiscan data (49). The structure was solved using direct methods and refined with full-matrix, least-squares procedures on F^2. Two symmetry unique but chemically equivalent ion pairs are located in the asymmetric unit. One disordered methylene chloride molecule of crystallization per unit cell was located away from the ion pairs. The disordered triflate anions and methylene chloride molecule were treated as diffused contributions (Squeeze/Platon) (50). Two *t*-Bu-iCN ligands (one on each cation) and one fppy ligand were located disordered in two positions with refined site occupancies of 65/35, 80/20, and 54/46, respectively. The structure displays disorder that cannot be satisfactorily modeled because of the subtle differences (<1 Å) in atomic positions leading to larger than ideal $U_{eq_{max}}/U_{eq_{min}}$ ranges, low C−C precision and Hirshfeld test failures. All bonds were restrained as rigid bonds with common U_{ij} values within standard deviation. All non-hydrogen atoms were refined with anisotropic displacement parameters. All hydrogen atoms were treated as idealized contributions. Structure factors are contained in the SHELXTL 6.12 program library (49). The structure has been deposited at the Cambridge Crystallographic Data Centre under CCDC 717607.

Determination of Oxygen Quenching Sensitivity (Q_S). The degree of bimolecular quenching is dependent upon the concentration of oxygen in the PSP which in turn is determined by air pressure according to Henry's law. The effect of the partial pressure of oxygen (pO_2) on PSP luminescence can be quantified by the Stern–Volmer relationship

$$\frac{I_0}{I} = 1 + k_q\tau_0[O_2] = 1 + K_{sv}(pO_2) \qquad (1)$$

where I_0 and I are luminescence intensity in the presence and absence of quencher, respectively, k_q is the quenching rate coefficient that is largely diffusion limited, τ_0 is the luminescence lifetime in the absence of quencher, and K_{SV} is the Stern–Volmer quenching constant. When measurements at zero oxygen concentrations are inconvenient (e.g., Wind tunnel experiments), an alternate point of reference (usually atmospheric pressure) is used. In this case, eq 1 becomes

$$\frac{I_{ref}}{I} = C + Q_s\frac{P}{P_{ref}} \qquad (2)$$

where P_{ref} is the reference pressure at which the luminescent compound's intensity is I_{ref} and C is normally $1 - Q_s$ if temperature is constant. The slope of the Stern–Volmer plot, Q_s is a measure of the luminescent compound's sensitivity to oxygen.

Each PSP formulation was applied to a primed aluminum plate with a Tristar Starpoxy fluid resistant white epoxy primer (DHMS C4.01 Ty3) using a conventional airbrush. It was then mounted in a pressure chamber described elsewhere (43, 44). The average film thickness was estimated to be 2 ± 1 μm by a Positector 6000 model thickness gauge. Excitation was provided by a Hamamatsu Lightningcure LC5 200W (model L8333 Hg–Xe) source via a 10 m × 8 mm Oriel UV–vis liquid light guide. Several optical filters in parallel were placed inside the lamp, before the light guide, to block wavelengths greater than 400 nm (Rapp Optoelectronic UV-1 and Hamamatsu A7028–05 filter). Thin-film emission spectra were collected using an Acton Research Corporation SpectruMM CCD detection system. A fiber optic lightguide (LG-455–020), equipped with a Kodak Wratten Gelatin 3 filter absorbing ultraviolet radiations passed the emission through a SpectraPro-150 imaging dual grating monochromator/spectrograph onto a 16-bit Hamamatsu 1024 × 256 CCD. Following the dark current subtraction, the spectra were normalized by the maximum intensity at atmospheric pressure to produce the spectra variations with pressure (I_{ref}/I). Data for the Stern–Volmer plots were obtained by integrating the spectra over wavelengths between 460 and 560 nm. These measurements were taken at 24 °C, between 0.007 and 45 psi. A Scanivalve Corp. pressure calibrator/controller and a thermoelectric cooler coupled to a temperature controller were used to control pressure and temperature, respectively. Measurements at the reference pressure of 14.7 psi were taken two times during the calibration in order to estimate the photostability of the paints. The excitation light source stability was monitored with a temperature controlled Oriel 7123 photodiode.

RESULTS AND DISCUSSION

Syntheses and Characterizations. The reaction of *tert*-butyl isocyanide with the chloride-bridged iridium dimer $[Ir(fppy)_2Cl]_2$, using a method similar to that of Li et al. (45)), gave complex **1** in 72% yield. The ^1H NMR spectrum of this complex was consistent with its formulation and the proton chemical shifts of 4-(2-pyridyl)benzaldehyde and *tert*-butyl isocyanide ligands were assigned on the basis of a COSY 2-D analysis (see Experimental Section and the Supporting Information). Single-crystal X-ray crystallographic analysis of **1** at 120 K determined its crystal structure and showed that two symmetry unique but chemically equivalent ion pairs are located in the asymmetric unit. Full data are given in the Supporting Information but here we present an ORTEP drawing of one iridium cation (Figure 1). Crystallographic data and some selected bond lengths and angles are given in Tables 1 and 2, respectively. In Figure 1, iridium occupies a distorted octahedral coordination sphere of four carbon and two nitrogen donor atoms in which *tert*-butyl isocyanide ligands are cis to each other. In this stereochemistry, the bidentate pyridylbenzaldehyde ligands are expected to be coordinated to iridium with pyridine nitrogens trans to each other because that is the geometry of the reagent dimer complex (51), which is unchanged by the synthesis of **1**. The Ir–N bond lengths (Table 2) are similar to those of analogous complexes possessing the bis(pyridyl-

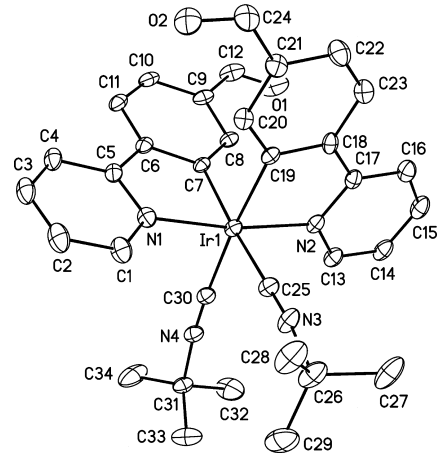

FIGURE 1. ORTEP of $1 \cdot 0.25(CH_2Cl_2)$ with thermal ellipsoids at the 30% probability level. The alternate disordered contribution, second symmetry unique ion pair, triflate counterion, methylene chloride solvent molecule, and hydrogen atoms are omitted for clarity.

Table 1. X-ray Crystallographic Data and Refinement Details for $1 \cdot 0.25(CH_2Cl_2)$

empirical formula	$C_{35}H_{34}F_3IrN_4O_3S \cdot 0.25(CH_2Cl_2)$
M_r	861.15
cryst syst	triclinic
space group	$P\bar{1}$
a (Å)	15.164(5)
b (Å)	17.083(6)
c (Å)	17.242(6)
α (deg)	117.569(5)
β (deg)	104.876(5)
γ (deg)	100.075(5)
V (Å^3)	3595(2)
D_x (g cm^{-3})	1.591
T (K)	120(2)
λ (Å)	0.71073
$R[F^2 > 2\sigma(F^2)]$	0.0498
$wR(F^2)$	0.1343
Z, Z'	4, 2
μ (mm^{-1})	3.864
GOf	1.034

Table 2. Selected Bond Lengths (Å) and Angles (deg) for $1 \cdot 0.25(CH_2Cl_2)$[a]

Ir1—N1	2.049(5), 2.039(10)	N1—Ir1—N2	170.7(2), 165.2(6)
Ir1—N2	2.047(5), 2.051(5)	C25—Ir1—C30	91.9(4). 89.1(3)
Ir1— C7	2.046(6), 2.057(11)	C7—Ir1—N1	80.1(2), 80.0(5)
Ir1—C25	2.037(8), 2.062(6)	C19—Ir1—N2	80.3(2), 79.9(2)
C12—O1	1.147(9), 1.148(14)	C25—Ir1—C30	91.94(4), 89.1(3)
C24—O2	1.202(8), 1.193(7)	N3—C25	1.138(10), 1.157(8)
N3—C26	1.515(13), 1.457(10)	N4—C30	1.164(8), 1.118(8)
N4—C31	1.487(9), 1.464(8)		

[a] The second value is for chemically equivalent bonds in the second symmetry unique cation. In case of disordered fragments, only the major contributor is represented.

Scheme 1

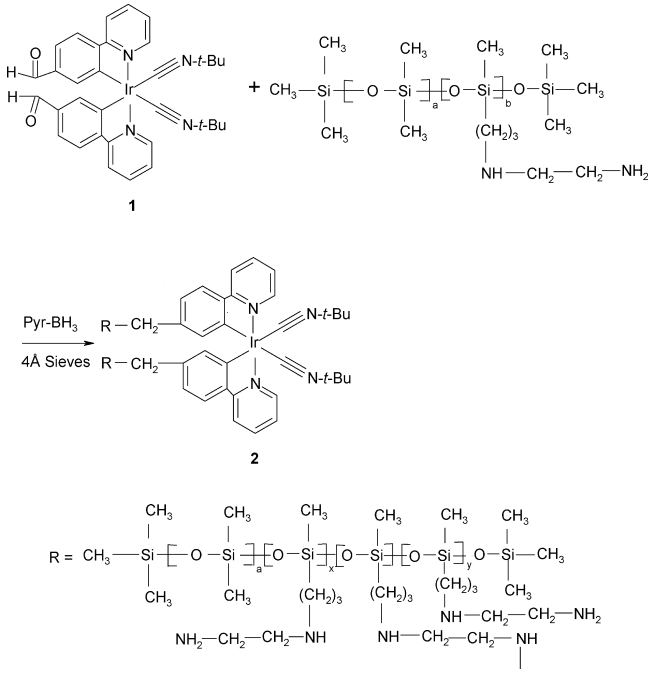

benzaldehyde)iridium fragment (47, 52). Figure 1 also shows that the *tert*-butyl isocyanide ligands are slightly bent, with Ir1—C30—N4 and C30—N4—C31 bond angles of 176.8(6) and 173.2(7)°, respectively, in agreement with those found in crystal structures of other *tert*-butyl isocyanide iridium complexes (53–57).

Reductive amination between **1** and the water-soluble amine-functionalized Silamine D208-EDA gave the luminophore-functionalized Silamine, **2,** as shown in Scheme 1.

The yield of the reaction in Scheme 1 was estimated by assuming that the electronic absorption properties of the iridium complex in **2** were the same as those of free complex **3**. Thus, a quantitative solution of **2** in CH_2Cl_2 showed a $\pi-\pi^*$ absorption band at 263 nm that was assumed to possess the same extinction coefficient as the $\pi-\pi^*$ absorption band of **3** ($\lambda = 260$ nm, $\varepsilon = 3.35 \times 10^4$ M^{-1} cm^{-1}). The calculated concentration of iridium complex in **2** indicated quantitative attachment of **1** to Silamine.

The attachment of **1** shown in Scheme 1 is of cross-linked Silamine chains. However, it is also possible for **1** to bind to a single Silamine chain by one or two methyl—amine links. There was no evidence of unreacted aldehyde in the ^{1}H NMR

Table 3. Solution Absorption,[a] Emission,[b] and Photophysical Data[b] for 1, 2, and 3

	1	2	3[c]
λ_{max} $\pi-\pi^*$(nm) (ε)[d]	258 (2.51×10^4)	239, 263, 317	260 (3.35×10^4)
λ_{max} MLCT (nm) (ε)	367 (6.92×10^3)	359	348 (1.21×10^4)
λ_{max} emission (nm)	496	461	458
ϕ	0.35	0.23	0.28
τ (μs)	17.3	20.6	35.6

[a] CH_3CN. [b] CH_2Cl_2. [c] From ref 10. [d] Units of M^{-1} cm^{-1}.

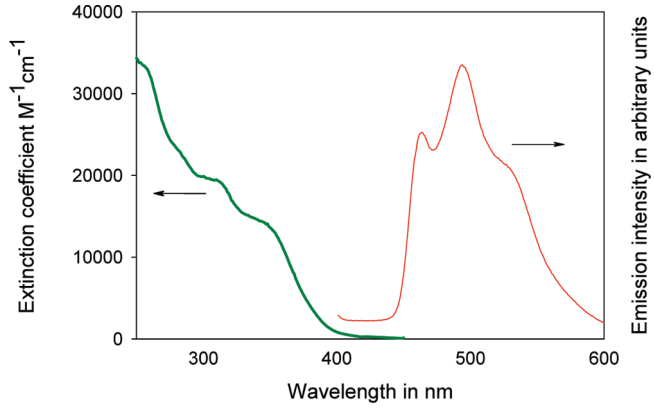

FIGURE 2. Solution absorption and emission spectra of 2. The absorption spectrum was acquired in CH_3CN and the emission spectrum was acquired in CH_2Cl_2. For 2, the extinction coefficient at $\lambda = 255$ nm was assumed to be identical with that of 3 at 260 nm. See Table 3 data.

of **2** (see the Supporting Information), which may indicate a complete condensation reaction or reduction of the aldehyde group by pyridine—borane. Unfortunately, ^{1}H NMR chemical shift of phenylpyridine protons overlaps with an imine proton that may be present. This, together with the large molecular weight of **2**, makes an assignment of the chemical shift of an imine proton ambiguous. Nevertheless, the similarity of **2** and **3**'s photophysical properties and electronic absorption spectroscopy (vide infra) suggests that imine linkages were reduced to methyl—amines by pyridine—borane. This was desired in order to closely match the electronic and photophysical properties of the Silamine bound iridium complex to those of complex **3.**

Electronic Spectroscopy and Photophysical Data. Room temperature absorption and emission data for **1**, **2**, and **3** have been placed in Table 3 and Figure 2 shows representative absorption and emission spectra of **2**. Three characteristic absorption bands are observed; the overlapping bands at $\lambda = 239$, 263, and 317 nm are assigned to fppy ligand $\pi-\pi^*$ transitions, whereas the band $\lambda = 359$ nm is assigned to iridium to fppy metal-to-ligand charge-transfer (MLCT) transitions (45, 47, 51, 58).

For **1**, the aldehyde group of the fppy ligand appears to decrease the extinction coefficient of the MLCT band and to shift it to longer wavelengths compared to the MLCT band of **3**. The decrease in MLCT intensity reflects a decrease in metal—ligand coupling (59) and the shift to longer wavelengths, particularly for emission, is consistent with a stabilization of the π^* orbitals of fppy by a conjugated electron-withdrawing substituent. In Figure 2, the emission band

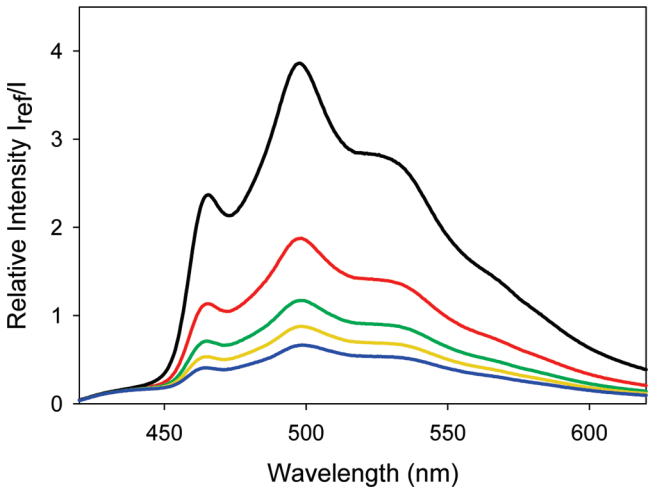

FIGURE 3. Effect of pressure on thin film luminescence of 2 in 1:2.3 Silamine:MC, P = 0.3 mbar, black; 0.34 bar, red; 1.00 bar, green; 1.70 bar, yellow; 2.72 bar, blue. I_{ref} is measured at 1 atm.

shows a vibronic progression that has been previously analyzed for a series of Ir(tolylpyridine)$_2$ complexes, assuming a dominant vibrational stretch (51). The relative intensities of these vibronic components is evidently substituent dependent as shown by the emission spectra of **1**, **2**, and **3** in acetonitrile (see the Supporting Information, Figure S2), but this was not investigated further. The photophysical data in Table 3 show that the excited MLCT state for each of these complexes is intensely emissive and possesses a long lifetime. These properties in combination with the oxygen quenching of the MLCT excited state find use in oxygen sensor applications.

Characterization of Presssure-Sensitive Paint (PSP) Films. Among the PSP films studied, the only completely water-soluble film formulations are those of **2**. The other film formulations required the addition of methanol to solubilize **1** and **3**. In addition, to compensate for the poor mechanical properties of Silamine D208-EDA, we included microcrystalline cellulose (MC) in the formulations. A representative study of the pressure-dependent film emission of **2** in 1:2.3 Silamine:MC is shown in Figure 3.

Films of **2** and **3** displayed an intense yellow-white luminescence with UV irradiation under low pressure conditions, while films of **1** showed a noticeably reduced luminescence despite having the same concentration of luminophore and a higher emission quantum yield (Table 3). This suggests that **1** aggregates and self-quenches in the film formulations used in this study. The decrease in emission intensity with increasing air pressure relative to the emission intensity at 1 atm pressure can be treated according to Stern–Volmer kinetics (see Experimental Section) and Figure 4 shows modified Stern–Volmer plots of **2** in three Silamine:MC formulations. A total of five Silamine:MC ratios were used for each luminophore in order to determine the conditions for optimum PSP performance. Oxygen quenching sensitivity data for all the films were calculated from linear fits to the Stern–Volmer plots with $r^2 > 0.95$ and have been placed in Table 4.

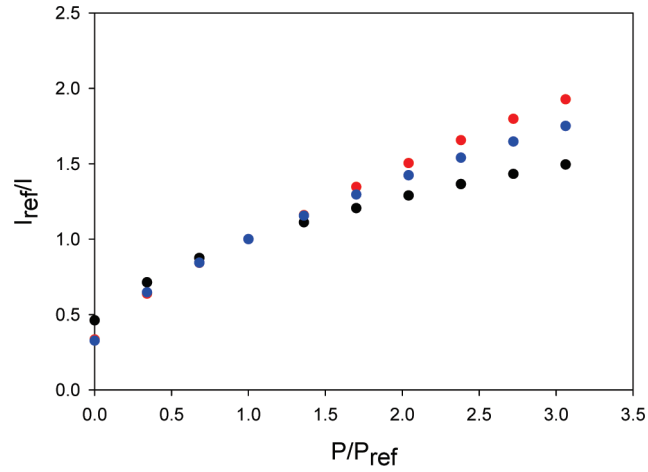

FIGURE 4. Room-temperature Stern–Volmer plots of 2 in 9:1 Silamine:MC, black; 1:1 Silamine:MC, red; 1:2.3 Silamine:MC, blue.

Table 4. PSP films Oxygen Sensitivities

luminophore	matrix	Q_s (r^2)
1	9:1 Silamine:MC	0.242 (0.973)[a]
	5:1 Silamine:MC	0.248 (0.977)[a]
	1:1 Silamine:MC	0.286 (0.974)[a]
	1:2.3 Silamine:MC	0.269 (0.970)[a]
	1:5 Silamine: MC	0.242 (0.974)[a]
2	9:1 Silamine:MC	0.277 (0.976)[a]
	5:1 Silamine:MC	0.277 (0.955)[a]
	1:1 Silamine:MC	0.502 (0.989)[b]
	1:2.3 Silamine:MC	0.439 (0.975)[b]
	1:5 Silamine:MC	0.327 (0.982)[a]
3	9:1 Silamine:MC	0.259 (0.992)[a]
	5:1 Silamine:MC	0.279 (0.991)[a]
	1:1 Silamine:MC	0.299 (0.980)[a]
	1:2.3 Silamine:MC	0.257 (0.981)[a]
	1:5 Silamine:MC	0.259 (0.975)[a]

[a] 5–45 psi. [b] 0.007–45 psi.

In most cases, the Stern–Volmer plots of thin films of **1**, **2** and **3** showed curvature in the low-pressure region (0.007 to 5 psi), which is probably a consequence of multiple quenching processes arising from hetereogenous luminophore environments. As seen from Figure 4 and the data in Table 4, quenching sensitivity (particularly for **2**) is dependent upon microcrystalline cellulose concentration. To help understand this, we examined the luminescence microscopy of films of **2**, and the results are shown in Figure 5.

In Figure 5A, luminescence microscopy shows that at low concentration of MC, the luminescence from the film is largely dispersed with some local enhancement around particles of MC. This localization of luminescence around MC particles becomes even more obvious in Figure 5B, the film that gives the best oxygen sensor performance. In Figure 5C, the film that has the greatest concentration of MC, an overall loss of luminescence intensity has obviously occurred which we attribute to light scattering by MC particles but there is still evidence of luminophore association with MC. It is suggested that the positively charged iridium luminophore

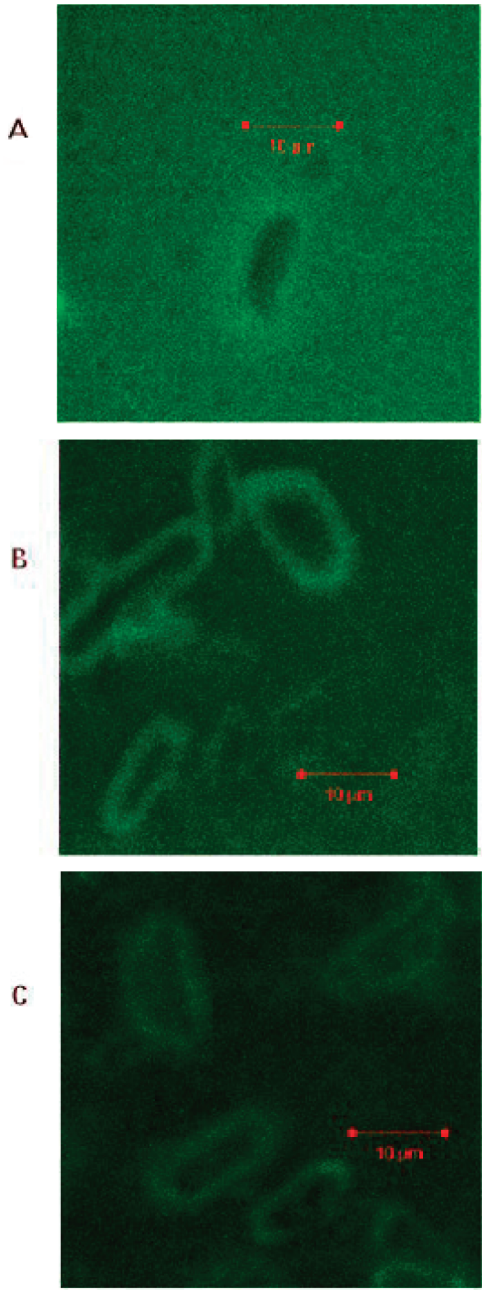

FIGURE 5. Luminescence microscopy of films of 2 performed under ambient conditions: (A) 9:1 Silamine:MC; (B) 1:1 Silamine:MC; (C) 1:5 Silamine:MC. The scale in red is 10 μm.

in **2** is electrostatically attracted to the polar groups on the surface of MC.

Lifetime measurements of 9:1, 1:1, and 1:5 Silamine:MC films of **2**, under ambient pressure and vacuum, are compiled in Table 5. Emission decay was fitted with a double exponential assuming two luminophore environments: **2** in Silamine polymer and **2** associated with the MC surface. The data show an increase in lifetime with increasing MC fraction. Quenching sensitivity Q_s is dependent upon both lifetime and the quenching rate constant k_q (eq 1 and 2) and so the observation of an optimum Q_s value (see Table 4) with MC fraction suggests that the quenching rate constant, or more specifically the diffusion of oxygen, must decrease with increasing fraction of MC (60). The optimum PSP

Table 5. Luminescence Lifetime Data of 2 in Silamine:MC Films in Microseconds

	vacuum			ambient pressure		
Silamine:MC film	τ_1	τ_2	R^2	τ_1	τ_2	R^2
9:1	0.5	5.9	0.990	0.3	4.9	0.986
1:1	0.6	17.6	0.995	0.6	12.9	0.997
1:5	3.2	25.8	0.993	0.5	15.3	0.984

formulation in Table 4 is **2** in 1:1 Silamine:MC, which gave an oxygen sensitivity of 0.502, with good linear behavior in a pressure range of 0.007 to 45 psi.

The temperature dependence of emission intensity of **1**, **2**, and **3** in 1:1 Silamine:MC films were examined in the temperature range of 10−40 °C under vacuum and 1 bar atmospheric pressure. The emission intensities were normalized to that at 10 °C and the results plotted in Figure 6.

In Figure 6, the data for the temperature dependence of emission gave good linear least-squares fits passing through or at least closely approaching the normalization value at 10 °C. The temperature sensitivities (percent intensity loss per degree) of the films were determined to be −1.5 and −1.6 % $°C^{-1}$ for **1**, −1.1 and −1.4 % $°C^{-1}$ for **2**, and −1.1 and −1.3 % $°C^{-1}$ for **3** at vacuum and 1 bar atmospheric pressure, respectively. The increase in temperature sensitivity at 1 bar atmospheric pressure relative to that at vacuum can be ascribed to the temperature dependence of bimolecular oxygen quenching and is expected but the significant temperature sensitivities of the films of **1**, **2**, and **3** in vacuum are not. Luminescence decay of $Ir(C_s)(acac)_2$, where Cs is 3-benzothiazol-2-yl)-7-(diethylamino)-coumarin and acac is acetylacetonate, showed very little dependence on temperature from 1 to 50 °C in vacuum (43). Similarly, PSP's using osmium complex luminophores have shown a range of temperature sensitivities varying from −0.11 to 1.00 % $°C^{-1}$ in vacuum (22), which suggests that the nature of the coordination sphere plays a critical role in determining temperature sensitivity. In any case, the temperature sensitivity of **2** in 1:1 Silamine:MC films must be compensated

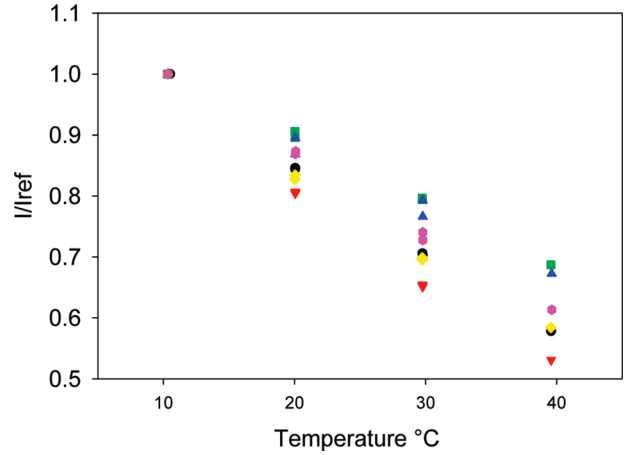

FIGURE 6. Temperature versus emission intensity ratio (I_{ref} is the intensity at 10 °C) of 1 in 1:1 Silamine:MC: vacuum, black circle; P = 1 bar, red triangle. 2 in 1:1 Silamine:MC: vacuum, green square; P = 1 bar, yellow diamond. 3 in 1:1 Silamine:MC: vacuum, blue triangle; P = 1 bar, purple circle.

for to obtain correct barometric data and this can be achieve by using a temperature sensitive calibrant as in a dual-luminophore oxygen and temperature sensor film (61).

CONCLUSIONS

The luminescent cyclometalated iridium complex $[Ir(fppy)_2(t\text{-}Bu\text{-}iCN)_2]CF_3SO_3$, **1**, was prepared and characterized and bound by reductive amination to the water-soluble amine-functionalized polymer Silamine D208-EDA, producing **2**, a water-soluble luminescent polymer. A PSP film of **2** in 1:1 Silamine:MC had an oxygen sensitivity of 0.502 over an atmospheric pressure range of 0.007−45 psi. Temperature sensitivity (percentage loss of intensity per °C) of this film was determined to be −1.1 and −1.4 % $°C^{-1}$ at vacuum and 1 bar atmospheric pressure, respectively. The PSP formulations of **2** were entirely water-based and offer an environmentally friendly alternative to nonaqueous PSP formulations.

Acknowledgment. We thank Dr. Wayne Z. Y. Wang (Carleton University) for the use of his equipment for acquiring the steady-state emission spectrum, Dr. Carlos Monreal (Agriculture and Agri-Food Canada) for luminescence microscopy, and Dr. J. C. Scaiano (University of Ottawa) for his assistance in collecting lifetime data. Financial support by the Natural Science and Engineering Research Council of Canada (NSERC) in the form of a Discovery Grant (R.J.C.) and by Ontario Graduate Scholarships in Science and Technology (OGSST) (A.H.) is appreciated.

Supporting Information Available: Figures showing the numbering scheme used in assigning the ^{1}H NMR of **1**, the ^{1}H NMR of **1**, the absorption spectra of **1** and **3**, emission spectra of **1**, **2** and **3**, the COSY spectrum of **1**, NMR spectra of Silamine D208-EDA, **1** dispersed in Silamine D208-EDA and **2** (PDF); crystallographic details (CIF). This material is available free of charge via the Internet at http://pubs.acs.org.

REFERENCES AND NOTES

(1) Burke, C. S.; Moore, J. P.; Wencel, D.; McEvoy, A. K.; MacCraith, B. D. *J. Biomed. Opt.* **2008**, *13*, 014027/1−7.
(2) Ergeneman, O.; Dogangil, G.; Kummer, M. P.; Abbott, J. J.; Nazeeruddin, M. K.; Nelson, B. J. *IEEE Sens. J.* **2008**, *8*, 29–37.
(3) Takeuchi, Y.; Amao, Y. In *Frontiers in Chemical Sensors: Novel Principles and Techniques*; Orellana, G., Moreno-Bondi, M. C., Eds.; Springer Series on Chemical Sensors and Biosensors; Springer: New York, 2005; Vol. 3, pp 303−322.
(4) DeRosa, M. C.; Hodgson, D. J.; Enright, G. D.; Dawson, B.; Evans, C. E. B.; Crutchley, R. J. *J. Am. Chem. Soc.* **2004**, *126*, 7619–7626.
(5) T. Liu, T.; J. P. Sullivan; J. P. *Pressure and Temperature Sensitive Paints*; Springer: Berlin, 2005.
(6) Hasumoto, H.; Imazu, T.; Miura, T.; Kogure, K. *J. Oceanogr.* **2006**, *62*, 99–103.
(7) Gillanders, R. N.; Tedford, M. C.; Crilly, P. J.; Bailey, R. T. *Anal. Chim. Acta* **2005**, *545*, 189–194.
(8) Orellana, G.; Garcia-Fresnadillo, D. In *Optical Sensors: Industrial, Environmental and Diagnostic Applications*; Narayanaswamy, R., Wolfbeis, O. S., Eds.; Springer Series on Chemical Sensors and Biosensors; Springer: New York, 2004; Vol. 1, pp 309−357.
(9) Guo, L.; Ni, Q.; Li, J.; Zhang, L.; Lin, X.; Xie, Z.; Chen, G. *Talanta* **2008**, *74*, 1032–1037.
(10) Jorge, P.; Caldas, P.; Da Silva, J. C. G.; Rosa, C.; Oliva, A.; Santos, J.; Farahi, F. *Fiber Integr. Opt.* **2005**, *24*, 201–225.
(11) Glazer, B. T.; Marsh, A. G.; Stierhoff, K.; Luther, G. W. *Anal. Chim. Acta* **2004**, *518*, 93–100.
(12) O'Mahony, F. C.; O'Riordan, T. C.; Papkovskaia, N.; Kerry, J. P.; Papkovsky, D. B. *Food Control* **2005**, *17*286–234.
(13) O'Mahony, F. C.; O'Riordan, T. C.; Papkovskaia, N.; Ogurtsov, V. I.; Kerry, J. P.; Papkovsky, D. B. *Packag. Technol. Sci.* **2004**, *17*, 225–234.
(14) Nock, V.; Blaikie, R. J.; David, T. *Proc. SPIE* **2008**, *6799*, 67990Y/1–10.
(15) Lin, L.; Xiao, L.-L.; Huang, S.; Zhao, L.; Cui, J.-S.; Wang, X.-H.; Chen, X. *Biosens. Bioelectron.* **2006**, *21*, 1703–9.
(16) Papkovsky, D. B.; Hynes, J.; Fernandes, R. *Proc. SPIE* **2005**, *5994*, 599406/1–9.
(17) Gao, F. G.; Fay, J. M.; Mathew, G.; Jeevarajan, A. S.; Anderson, M. M. *J. Biomed. Opt.* **2005**, *10*, 054005/1−6.
(18) Kwok, N.-Y.; Dong, S.; Lo, W.; Wong, K.-Y. *Sens. Actuators, B* **2005**, *B110*, 289–298.
(19) Gao, F. G.; Jeevarajan, A. S.; Anderson, M. M. *Biotechnol. Bioeng.* **2004**, *86*, 425–433.
(20) Cheng, Y.; Samia, A. C.; Meyers, J. D.; Panagopoulos, I.; Fei, B.; Burda, C. *J. Am. Chem. Soc.* **2008**, *130*, 10643–10647.
(21) Brinas, R. P.; Troxler, T.; Hochstrasser, R. M.; Vinogradov, S. A. *J. Am. Chem. Soc.* **2005**, *127*, 11851–11862.
(22) Carlson, B.; Bullock, J. P.; Hance, T. M.; Phelan, G. D. *Anal. Chem.* **2009**, *81*, 262–267.
(23) Saerner, G.; Goeransson, U.; Linden, J.; Richter, M.; Alden, M. *Meas. Sci. Technol.* **2008**, *19*, 085307/1−6.
(24) Gregory, J. W.; Asai, K.; Kameda, M.; Liu, T.; Sullivan, J. P. *Proc. Inst. Mech. Eng., Part G* **2008**, *222*, 249–290.
(25) Huang, C.; Gregory, J. W.; Nagai, H.; Asai, K.; Sullivan, J. P. *Micro-Electro-Mech. Syst.* **2007**, *8*, 577–583.
(26) Lee, S. J.; Kang, J. H. *J. Visualization* **2006**, *9*, 137–144.
(27) Nagai, H.; Naraoka, R.; Sawada, K.; Asai, K. *AIAA J.* **2008**, *46*, 215–222.
(28) Guerrero-Viramontes, J. A.; Moreno Hernandez, D.; Mendoza Santoyo, F.; Moran Loza, J. M.; Garcia Arreola, A. *Proc. SPIE* **2007**, *6422*, 64220H/1–6.
(29) Yamashita, T. Y.; Sugiura, H.; Nagai, H.; Asai, K.; Ishida, K. *J. Visualization* **2007**, *10*, 289–298.
(30) Huang, C.; Gregory, J. W.; Sullivan, J. P. *J. Microelectromech. Syst.* **2007**, *16*, 777–785.
(31) Matsuda, Y.; Mori, H.; Niimi, T.; Uenishi, H.; Hirako, M. *Exp. Fluids* **2007**, *42*, 543–550.
(32) Castaldo, A.; Massera, E.; Quercia, L.; Di Francia, G. *Sens. Actuators, B* **2006**, *118*, 328–332.
(33) Mitsuo, K.; Asai, K.; Takahashi, A.; Mizushima, H. *Meas. Sci. Technol.* **2006**, *17*, 1282–1291.
(34) Kimura, F.; Khalil, G.; Zettsu, N.; Xia, Y.; Callis, J.; Gouterman, M.; Dalton, L.; Dabiri, D.; Rodriguez, M. *Meas. Sci. Technol.* **2006**, *17*, 1254–1260.
(35) Mori, H.; Niimi, T.; Hirako, M.; Uenishi, H. *Meas. Sci. Technol.* **2006**, *17*, 1242–1246.
(36) McGraw, C. M.; Bell, J. H.; Khalil, G.; Callis, J. B. *Exp. Fluids* **2006**, *40*, 203–211.
(37) Kameda, M.; Tabei, T.; Nakakita, K.; Sakaue, H.; Asai, K. *Meas. Sci. Technol.* **2005**, *16*, 2517–2524.
(38) Köse, M. E.; Omar, A.; Virgin, C. A.; Carroll, B. F.; Schanze, K. S. *Langmuir* **2005**, *21*, 9110–9120.
(39) Köse, M. E.; Carroll, B. F.; Schanze, K. S. *Langmuir* **2005**, *21*, 9121–9129.
(40) Obata, M.; Tanaka, Y.; Araki, N.; Hirohara, S.; Yano, S.; Mitsuo, K.; Asai, K.; Harada, M.; Kakuchi, T.; Outsuki, C. *J. Polym. Sci., Part A: Polym. Chem.* **2005**, *43*, 2997–3006.
(41) Oglesby, D. M.; Ingram, J. L.; Jordan, J. D.; Watkins, A. N.; Leighty, B. D. *NASA/TM* **2004**, *2004−213268*, 1–8.
(42) Köse, M. E.; Crutchley, R. J.; DeRosa, M. C.; Ananthakrishnan, N.; Reynolds, J. R.; Schanze, K. S. *Langmuir* **2005**, *21*, 8255–8262.
(43) DeRosa, M. C.; Mosher, P. J.; Evans, C. E. B.; Crutchley, R. J. *Macromol. Symp.* **2003**, *196*, 235–248.
(44) DeRosa, M. C.; Mosher, P. J.; Yap, G. P. A.; Focsaneanu, K.-S.; Crutchley, R. J.; Evans, C. E. B. *Inorg. Chem.* **2003**, *42*, 4864–4872.
(45) Bomann, M. D.; Guch, I. C.; DiMare, M. *J. Org. Chem.* **1996**, *60*, 5995–5996.
(46) Li, J.; Djurovich, P. I.; Alleyne, B. D.; Yousufuddin, M.; Ho, N. N.; Thomas, J. C.; Peters, J. C.; Bau, R.; Thompson, M. E. *Inorg. Chem.* **2005**, *44*, 1713–1727.
(47) Lo, K. K.-W.; Chung, C.-K.; Zhu, N. *Chem.—Eur. J.* **2003**, *9*, 475–483.
(48) Jones, G.; Jackson, W. R.; Choi, C.-Y.; Bergmark, W. R. *J. Phys. Chem.* **1985**, *89*, 294–300.

(49) Sheldrick, G. *SADABS and SHELXTL*; Bruker-AXS Inc; Madison, WI, 2001.
(50) Spek, A. L. *J. Appl. Crystallogr.* **2003**, *36*, 7–13.
(51) Lamansky, S.; Djurovich, P.; Murphy, D.; Abdel-Razzaq, F.; Kwong, R.; Tsyba, I.; Bortz, M.; Mui, B.; Bau, R.; Thompson, M. E. *Inorg. Chem.* **2001**, *40*, 1704–1711.
(52) Chen, H.; Zhao, Q.; Wu, Y.; Li, F.; Yang, H.; Yi, T.; Huang, C. *Inorg. Chem.* **2007**, *46*, 11075–11081.
(53) Tejel, C.; Ciriano, M. A.; Lopez, J. A.; Lahoz, F. J.; Oro, L. A. *Organometallics* **2000**, *19*, 4977–4984.
(54) Tejel, C.; Ciriano, M. A.; Lahoz, F. J.; Oro, L. A. *Organometallics* **1998**, *17*, 1449–1451.
(55) Dobbs, D. A.; Bergman, R. G. *Inorg. Chem.* **1994**, *33*, 5329–5336.
(56) Mague, J. T. *Polyhedron* **1992**, *11*, 677–686.
(57) Maverick, A. W.; Smith, T. P.; Maverick, E. F.; Gray, H. B. *Inorg. Chem.* **1987**, *26*, 4336–4341.
(58) Nazeeruddin, M. K.; Humphry-Baker, R.; Berner, D.; Rivier, S.; Zuppiroli, L.; Graetzel, M. *J. Am. Chem. Soc.* **2003**, *125*, 8790–8797.
(59) Tamayo, A. B.; Alleyne, B. D.; Djurovich, P. I.; Lamansky, S.; Tsyba, I.; Ho, N. N.; Bau, R.; Thompson, M. E. *J. Am. Chem. Soc.* **2003**, *125*, 7377–7387.
(60) Puklin, E.; Carlson, B.; Gouin, S.; Costin, C.; Green, E.; Ponomarev, S.; Tanji, H.; Gouterman, M. *J. Appl. Polym. Sci.* **2000**, *77*, 2795–2804.
(61) Köse, M. E.; Omar, A.; Virgin, C. A.; Carroll, B. F.; Schanze, K. S. *Langmuir* **2005**, *21*, 9110–9120.

AM900306A